Journal of the Iranian Chemical Society
https://doi.org/10.1007/s13738-020-01853-x

ORIGINAL PAPER

Structural chemistry and anti-inflammatory activity of flexible/restricted phenyl dimers

Ved Prakash Singh[1] · Jayanta Dowarah[1] · Ashish Kumar Tewari[2] · David K. Geiger[3]

Received: 21 August 2019 / Accepted: 2 January 2020

Abstract

Three phenyl dimer compounds, namely 3,3′-Diformyldiphenoxyethane ($C_{16}H_{14}O_4$) (**1**), 1-(4-[2-(4-Acetyl-phenoxy)-ethoxy]-phenyl)-ethanone ($C_{17}H_{16}N_2O_3$) (**2**), 1-{4-[2-(4-Acetyl-phenoxymethyl)-benzyloxy]-phenyl}-ethanone ($C_{24}H_{22}O_4$) (**3**), were obtained and fully characterized, including their crystal structure determinations. The structural properties of two compounds 4, 4′-(ethylenedioxy)dibenzaldehyde) ($C_{16}H_{14}O_4$) (Marriott et al. J Med Chem 42:3210, 1999) [1] (**4**) and 4-(2-Phenoxy-ethoxy)-benzaldehyde ($C_{15}H_{14}O_3$) (Hunter, Chem Soc Rev 23:101, 1994) [2] (**5**) are discussed with the role of the substituent in crystal packing. In vivo, anti-inflammatory activities of all compounds were studied on Wistar strain albino rats. All the compounds exhibited anti-inflammatory activity except **5**. Compounds **1, 2, 4** have shown moderate-to-intermediate effects on inhibitory properties. Compound (**3**) with restricted rotation in the compound-like SC-558 drug was shown to possess good inhibitory properties at 180 min. In silico analysis was performed and compared with experimental in vivo results.

Keywords Weak interactions · Anti-inflammatory activity · Docking · Interaction energy

Introduction

Non-covalent interactions are significant in drug design and the biological activity of compounds. It is also essential in the strategic design of bioactive solid materials with desirable architectures. Structural biology and X-ray crystallography had provided beneficial information in the development of new drugs. It already established that for good activity and selectivity, compounds should have key pharmacophore [3]. Several kinds of forces play an essential role in the binding of a particular drug to particular receptors. Aromatic interactions non-covalent interactions play a subtle role in drug–receptor binding mechanisms. Since the majority of biologically active compounds consists of aromatic and hetero-aromatic units, which provide an opportunity for weak interactions such as C–H···π, and π–π types of non-conventional H-bonds [4, 5]. Aromatic interactions are neither too strong nor too weak by nature, but these are enough to retain the stable drug–receptor complex [6–8]. Therefore, these interactions are significant in drug design and development of the drug.

A literature survey revealed [9–11] that many 1,2 and 1,3-diaryl heterocycle fleximers have found their clinical application as NSAIDs, and are good COX-2 inhibitors [12, 13] Sometimes five-membered rings link these and are situated at 1, 2 positions of five-membered rings like SC-558. According to the Gold hypothesis, two rings were inserted in two pockets of COX-2 enzyme and interact with Tyr-355, Arg-120, and Phe-518 as well as with one hydrogen bond that involved the $-SO_2CH_3$ group with Tyr-115, Arg-513 [14]. According to the structure–activity relationship and topology of the COX-2 active site, the inhibitors of the

Electronic supplementary material The online version of this article (https://doi.org/10.1007/s13738-020-01853-x) contains supplementary material, which is available to authorized users.

✉ Ved Prakash Singh
vpsingh@mzu.edu.in

✉ Ashish Kumar Tewari
tashish2007@gmail.com

David K. Geiger
geiger@geneseo.edu

[1] Department of Chemistry, School of Physical Sciences, Mizoram University, Aizawl 796004, India

[2] Department of Chemistry, Institute of Science, Banaras Hindu University, Varanasi 221005, India

[3] Department of Chemistry, College of Genesco, State University of New York, Genesco, NY 4454, USA

Published online: 13 January 2020

enzyme should consist of at least an H bond acceptor, two aromatic rings, and two hydrophobic groups [14].

As per in silico analysis, the flexibility of the compound can increase the compatibility of the compound to fit in the pocket of the COX-2 enzyme [13]. Motivated by the findings mentioned above, we have synthesized a series of diaryl systems attached to C-1 and C-2 of the ethane nucleus and substituted ethane system. These molecules are motivated by the restricted rotation of SC-558 as well as flexible drugs such as Rofecoxib and Porecoxib. In one of the compounds, phenyl ring is introduced to reduce the flexibility of the compound. In the rest of the compounds, flexibility is high to make it more compatible to fit in the pocket of COX-2. In this series of the compound, CHO and $COCH_3$ groups are introduced in the ring to make hydrogen bonding with active site at COX-2 like SC-558. These groups are introduced as a hydrogen bond acceptor. The position of CHO groups varied from meta- to para-positions to observe the most effective position in molecular binding with COX-2 active site. In one of the designed molecules, only one ring is substituted with the –CHO group motivated by Rofecoxib and Porecoxib [14].

These compounds have different functional groups to provide polarized structure to make C–H···π, π–π, and other weak interactions as per requirement for drug action. These analogs have flexibility as well as multiple sites to develop proximity for weak interactions with receptor sites with good potential. We have selected these compounds for screening as anti-inflammatory agents based on rationale celecoxib, the 1,2-diaryl compound, which is COX-2 selective drug. In the present series of the compound, we explore the structural property of five compounds with different degrees of freedom, which may be useful to study for binding of the molecules with the target receptor in various conditions. The results of the structural exploration of the different weak interactions, including the Hirshfeld surface analysis, are reported with in silico analysis and *in vivo* activity analysis of all the fleximers.

Experimental

Synthesis and crystallization

Synthesis of 3, 3′-Diformyldiphenoxyethane (1)

In a 100-ml round-bottom flask, *m*-hydroxybenzaldehyde (3 g, 0.025 mol) and potassium carbonate (3.4 g, 0.0025 mol) were taken in DMF and stirred for 20 min. After 20 min, 1, 2-dibromoethane was added and stirred. The completion of reaction was checked via TLC (20% EtOAc & Hexane), in which one spot visualized. After completion of the reaction, DMF removed under through rotary evaporator and the reaction mixture extracted with $CHCl_3$. The $CHCl_3$ layer was dried with anhydrous Na_2SO_4 and filtered. The product recovered from $CHCl_3$, and the product was purified via crystallization. It was characterized as compound 2; it was recrystallized *via* diffusion of hexane into an ethyl acetate at room temperature.

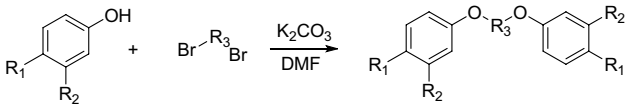

Compound 1	R_1= H, R_2= CHO, R_3= -CH_2CH_2-
Compound 2	R_1= $COCH_3$, R_2= H, R_3= -CH_2CH_2-
Compound 3	R_1= $COCH_3$, R_2= H, R_3= o-$CH_2C_6H_5CH_2$-
Compound 4	R_1= CHO, R_2= H, R_3= -CH_2CH_2-

General Scheme for compound 1-4

(**1**); Yield: 1.81 g, 49%. Mp.113-15°C.

^{1}H NMR 300 MHz, 25 °C, Si(CH_3)$_4$, ($CDCl_3$) (δ): 4.24 (4H, s, 2OC<u>H</u>$_2$); 7.23 (2H, s, Ar-H), 7.45–7.49 (6H, d, Ar-H, J = 11.4 Hz) 9.98 (2H, s, –C<u>H</u>O). **^{13}C NMR (75 MHz, $CDCl_3$):** (δ): 64.67, 114.69, 114.99, 117.96, 130.22, 163.36, 163.62, 190.78. **MS (m/z):** 271 (M + 1). **Element Analysis: (i). Calculated:** C = 71.11%; H = 5.17%. **(ii). Found**: C = 71.15%; H = 5.11%.

Synthesis of 1-{4-[2-(4-Acetyl-phenoxy)-ethoxy]-phenyl} -ethanone (2)

In a 100-ml round-bottom flask, p-hydroxy acetophenone (2 g, 0.015 mol) and potassium carbonate (2.3 g, 0.015 mol) were taken in DMF and stirred for 20 min. After 20 min, 1,2-dibromoethane was added and stirred it for 12 h. Completion of the reaction was checked via TLC (20% EtOAc & Hexane) in which one spot visualized. After completion of the reaction, DMF removed under reduced pressure through the rotary evaporator, and the reaction mixture was extracted with $CHCl_3$/ H_2O (200/200 × 3 ml). The $CHCl_3$ layer was dried with anhydrous Na_2SO_4 and filtered. Chloroform was removed, and the product was purified via crystallization. A single crystal was obtained via slow evaporation of a solution of the product in ethyl acetate at room temperature.

(**2**); Yield: 1.41 g, 67%.Mp.132-34 °C.

^{1}H NMR 300 MHz, 25 °C, Si(CH_3)$_4$, ($CDCl_3$) (δ): 2.57 (6H, s, 2C<u>H</u>$_3$); 4.42 (4H, s, OC<u>H</u>$_2$); 6.87–6.90 (4H, *d*, Ar-<u>H</u>, J = 8.1 Hz); 7.92–7.95 (4H, *d*, Ar-<u>H</u>, J = 8.1 Hz). **^{13}C NMR (75 MHz, $CDCl_3$):** (δ): 26.20, 68.49, 111.48, 123.56, 130.69, 133.31, 162.36, 196.62. **MS (m/z):** 299.4 (M + 1).**Element Analysis: (i). Calculated:** C = 70.07%; H = 6.57. **(ii). Found**: C = 69.99%; H = 6.59%.

Synthesis of 1-{4-[2-(4-Acetyl-phenoxymethyl)-benzyloxy]-phenyl}-ethanone (3)

In a 100-ml round-bottom flask, p-hydroxy acetophenone (2 g, 0.015 mol) and potassium carbonate were taken and stirred for 20 min. After 20 min, 1,2-dibromoxylene was added and stirred. The completion of reaction was checked via TLC (20% EtOAc & Hexane), in which one spot visualized. After completion of the reaction, DMF removed under reduced pressure, and the reaction mixture was extracted with $CHCl_3/H_2O$. The $CHCl_3$ layer was dried and filtered. The product was purified via crystallization. A single crystal was obtained via slow evaporation in ethyl acetate at room temperature.

(**3**); Yield: 1.80 g, 80%.Mp.141-43 °C.

^{1}H NMR 300 MHz, 25 °C, Si(CH_3)$_4$, ($CDCl_3$) (δ): (δ): 2.55 (6H, s, 2C$\underline{H}_3$); 5.23 (4H, s, 2OC$\underline{H}_2$); 6.97–7.00 (4H, *d*, Ar-$\underline{H}$, J = 8.7 Hz), 7.39–7.42 (2H, m, Ar-$\underline{H}$); 7.50–7.53 (2H, m, Ar-$\underline{H}$); 7.90–7.93 (4H, *d*, Ar-$\underline{H}$, J = 9.0 Hz). **^{13}C NMR (75 MHz, $CDCl_3$):** (δ): 26.27, 68.14, 114.38, 128.74, 129.16, 130.56, 130.69, 134.39, 162.28, 196.56. **MS (m/z):** 374 (M + 1).**Element Analysis: (i). Calculated:** C = 77.01%; H = 5.88%. **(ii). Found**: C = 77.10%; H = 5.89%.

Synthesis of 4, 4′-Diformyldiphenoxyethane (4) [1]

.

Synthesis of 4-(2-Phenoxy-ethoxy)-benzaldehyde (5) [2]

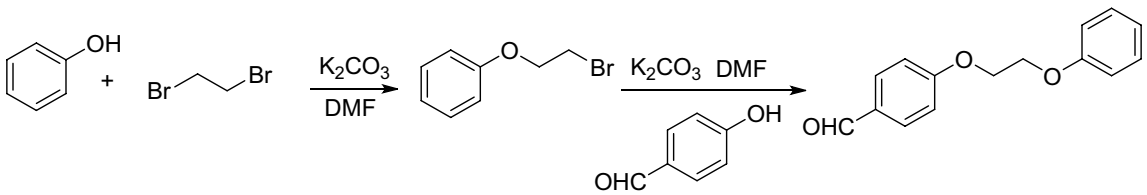

Scheme for compound 5

Crystal structure determination and Hirshfeld surface analysis

X-ray crystallography

Single-crystal X-ray data for compounds (1) and (2) and 3 were collected with an Oxford Diffraction Xcalibur CCD diffractometer. Crystallographic details of compounds **1, 2**, and **3** are summarized in Table 1.

Hirshfeld Surface, finger-plot and weak interaction energy analysis

The Hirshfeld surface analysis was performed by using *CrystalExplorer 17* [20] to explore the space occupied by a molecule in the crystalline solid-state to know the electron density into the molecule. The fingerprint plot of the molecules was used to explore the packing modes and non-covalent interactions in the molecule. Interaction energies for (3) were calculated employing the CE-B3LYP/6-31G(*d*,*p*) functional/basis set combination and are corrected for basis set superposition energy (BSSE) using the counterpoise (CP) method [21]. The interaction energy is broken down as

$$E_{tot} = k_{ele}E'_{ele} + k_{pol}E'_{pol} + k_{dis}E'_{dis} + k_{rep}E'_{rep},$$

where the k values are scale factors, E'_{ele} represents the electrostatic component, E'_{pol} the polarization energy, E'_{dis} the dispersion energy, and E'_{rep} the exchange–repulsion energy [22, 23]. The C–H bond lengths converted to normalized values based on neutron diffraction results [24]. A preliminary analysis of important intermolecular interactions was performed using *PLATON* [25].

COX-2 interaction in silico analysis and evaluation of the anti-inflammatory effects of compounds (1)–(5)

In silico analysis

The ability of compounds to interact with the COX-2 was assessed by in silico studies. Here for docking, PDB ID 6cox was used to dock each compound to study the binding and

Table 1 Experimental detail

Compound crystal data	1 (CCDC 1906450)	2 (CCDC 1907007)	3(CCDC 1906456)
Chemical formula	C16H14O4	C18H18O4	C24 H22 O4
Mr	270.27	298.32	374.41
Crystal color	Yellowish	Colorless	Yellowish
Temperature	293(2) K	296(2) K	293(2) K
Wavelength	0.71073 Å	0.71073 Å	0.71073 Å
Crystal system, space group	Monoclinic, $P2_1/c$	Monoclinic, $P2_1/c$	Monoclinic, C2/c
a, b, c (Å)	5.6289(3), 16.0475(8), 7.3064(3)	9.1687(7), 5.5014(3), 15.1170(10)	13.0860(11), 10.4392(10), 14.3196(11)
α, β, γ	90.00°, 99.190(4), 90.00°	90.00°, 100.586(7)°, 90.00°	90.00°, 92.465(7) 90.00°
Cell volume, *V*	651.51(6) Å^3	749.53 (9) Å^3	1954.4(3)
Radiation type	MoKα	MoKα	MoKα
μ (mm^{-1})	0.099	0.09	0.086
Data collection diffractometer	Bruker APEX-II CCD	Bruker APEX-II CCD	Bruker APEX-II CCD
Absorption correction	Multi-Scan	Multi-Scan	Multi-Scan
T_{min}, T_{max}	0.95180, 1.00000	0.981, 0.988	0.940–1.000
No. of measured, independent and observed [$I > 2\sigma$(I)] reflections	2693, 1447, 1240	5176, 1759, 1261	4087, 2206, 1541
No. of reflections	1447	1759	2206
No. of parameters	92	101	128
No. of restraints	0	0	0
H-atom treatment	H-atom parameters constrained	H-atom parameters constrained	H-atom parameters constrained
F(000)	284	316	792.0
Crystal size	0.26 × 0.24 × 0.21 mm	0.19 × 0.16 × 0.12 mm	0.28 × 0.25 × 0.23 mm
Z	2	2	4
R factor (%)	3.33	3.78	4.14
Theta range for data collection	2.538–28.801	2.26–28.78	2.490–28.696
Limiting indices	$-7 \le h \le 7$, $-20 \le k \le 19$, $-9 \le l \le 4$	$-14 \le h \le 9$, $-11 \le k \le 10$, $-20 \le l \le 13$	$-17 \le h \le 12$, $-13 \le k \le 13$, $-13 \le l \le 18$
Melting point	352 K	408 K	417 K
R_{int}	0.010	0.015	0.14
(sin θ/λ)max (Å^{-1})	0.678	0.678	0.677
Final *R* indices [$F^2 > 2\sigma(F^2)$], wR(F^2), S	0.033, 0.097, 1.09	0.038, 0.104, 1.07	0.041, 0.119, 1.05
R indices (all data)	$R_1 = 0.0830$, $wR_2 = 0.1650$	$R_1 = 0.0548$, $wR_2 = 0.1044$	$R_1 = 0.0623$, $wR_2 = 0.1192$
$\Delta\rho_{max}$, $\Delta\rho_{min}$ (e Å^{-3})	0.29, −0.16	0.15, −0.18	0.18, −0.16

Computer programs: Bruker APEX2 [15], Bruker SAINT [16], SHELXT 2014 [17], SHELXL2014 [18], Bruker SHELXTL, and publCIF [19]

active site of drugs with COX-2 [26]. All the compounds were docked at the active site using Autodock-1.5.6, and PyMOL is used for visualization of the docked ligand–protein complex.

Evaluation of the anti-inflammatory effects of compounds

All experiments have been conducted on adult Wistar strain albino rats, weighing between 150 and 200 g. The animals were taken from the Central Animal House of the IMS, B.H.U. They kept under identical housing conditions at an ambient temperature of 25 °C ± 2 °C in colony cages and 45–55% relative humidity with the light–dark cycle in the departmental animal room. Carrageenin-induced paw edema [27] was used throughout the experiment.

Results and discussion

Compounds (1) and (2) crystallized in the monoclinic space group $P2_1/c$ with $Z = 2$, and compound 4 crystallized in the monoclinic space group Cc with $Z = 4$, whereas compound (5) crystallized in the monoclinic space group $P2_1/n$ with $Z = 4$. Compound (3) (density 1.273) is also having a similar kind of chemical environment with restricted rotation and

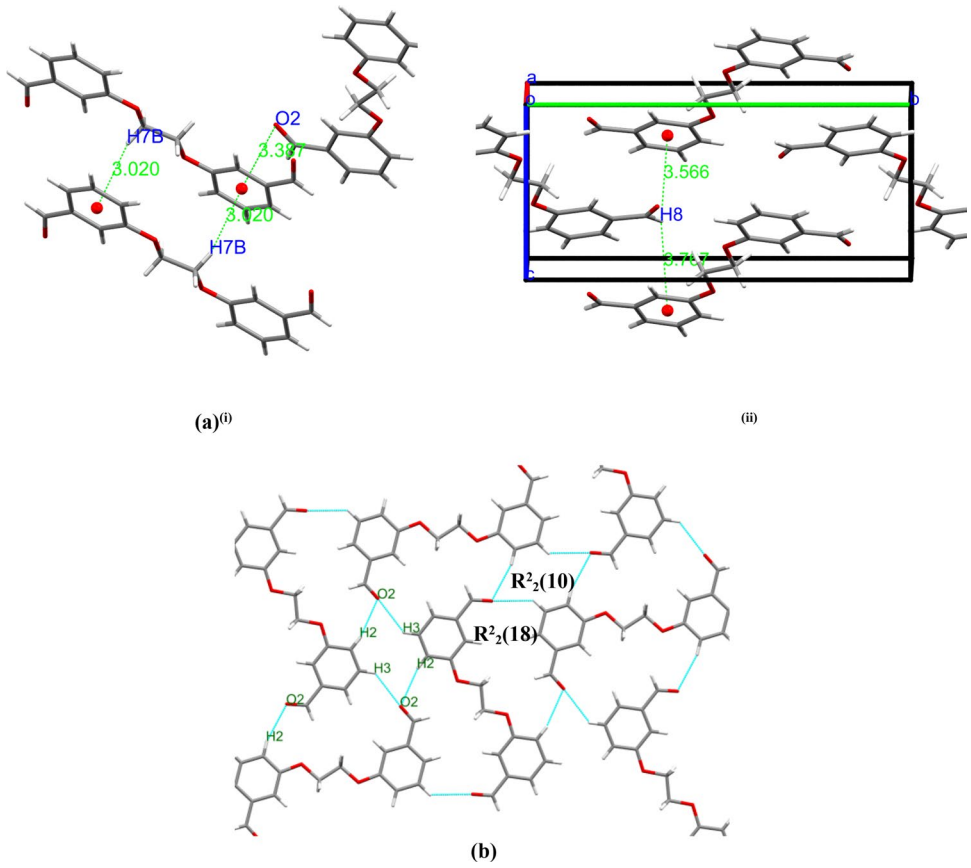

Fig. 1 Part of the crystal structure of compound (1), **a** (i) CH…π interactions, loan pair…π interactions (ii) Crystal packing view along a* and CH…π interactions **b** showing the formation of a hydrogen-bonded sheet lying parallel to (101) symmetry codes: (i) $-1+x,y,z$, (ii) $1-x, -1/2+y, 1.5-z$

crystallizes in the monoclinic, $C2/c$ space group with $Z=4$. Compounds (1), (2) and (4) are symmetrical fleximers, but substituted O-phenyl ring in compound s(1) and (2) are having staggered conformation at substituted ethane (linker of dimer), whereas compound (4) crystallized in gauche conformation due to intramolecular hydrogen bonding. Compound (5) is an unsymmetrical phenyl dimer, but it is also crystallized exactly like compound (4) in gauche conformation around the dimethylene linker. Compound (3) crystallized like V shape, and both the phenyl rings were orientated in the opposite face. Overall, the structure of compounds (1) and (2) (both rings are in the same plane) is quite similar in the crystalline phase. Compounds (4) and (5) both are having similarity in molecular structure in solid-state that is irrespective of symmetrical and unsymmetrical nature of the dimer.

The hydrogen-bonding network for (1) and crystal packing is shown in Fig. 1. In compound (1), both formyl group oxygens of the molecule are involved in hydrogen bonding, whereas linker oxygens are not involved in any weak interactions. In addition to C–H…O interactions in the extended structure of compound (1) are having intermolecular

Table 2 Hydrogen-bond geometry (Å) for (**1**)

D-H…A	D-H	H…A	D….A	D-H..A (°)
C2–H2…O2$^{(i)}$	0.929	2.538	3.436	162.38
C3–H3…O2$^{(ii)}$	0.930	2.552	3.280	135.53
C7–H7A…O2$^{(iii)}$	0.970	2.681	3.631	166.54
C8O2…Cg (C3 C2 C1 C6 C5 C4)$^{(iii)}$	1.210	3.387	3.498	84.66
C7–H7B…. Cg (C3 C2 C1 C6 C5 C4)$^{(iv)}$	0.970	3.020	3.931	156.98
C8–H8…. Cg (C3 C2 C1 C6 C5 C4)$^{(v)}$	0.929	3.566	3.489	87.18
C8–H8…. Cg (C3 C2 C1 C6 C5 C4)	0.929	3.767	4.092	63.30

Cg is the centroid of the ring

Symmetry codes: (i) $-$x, $-1/2+y$, ½$-z$ (ii) $-x, -1/2+y, 1/2-$z (iii) $1-x, -1/2+y, 1/2-$z (iv) $1-$x, $-1/2+y, 1.5-$z (v) $-1+x,y,z$

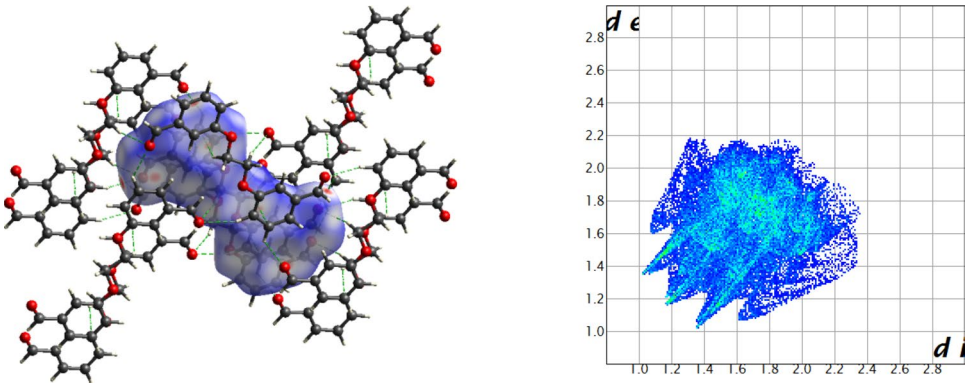

Fig. 2 Hirshfeld and fingerprint plots of compound (1)

Table 3 Interaction energies (kJ mol^{-1}) calculated for (**1**)

Interaction(s)	E'_{ele}	E'_{pol}	E'_{dis}	E'_{rep}	E_{tot}
2 C7–H7B…Cg(1)	−11.8	−1.8	−46.6	27.9	−37.2
C2–H2…O2/ C3-H3…O2 [$R^2_2(18)$]	−15.7	−4.5	−19.3	21.8	−23.3
C8–O8…Cg(1)	−7.1	−2.0	−27.5	19.2	−21.1
	−1.2	−0.4	−18.5	9.0	−12.2
	1.5	−0.6	−7.3	4.1	−2.7

Scale factors used to determine E_{tot}:k_{ele} = 1.057, k_{pol} = 0.740, k_{dis} = 0.871, and k_{rep} = 0.618 [16]. See "Hirshfeld surface, finger-plot and weak interaction energy analysis" for calculation details

loan-pair-π interactions between –CH=O and pi-electrons of the ring. In this compound, C–H…π interactions are exhibited in the crystal packing between C7H7b and pi-electrons of the ring of the adjacent molecule (Table 2). The aromatic ring is behaving as donor as well as an acceptor in C–H…π and loan pair interactions, respectively [22].

Hirshfeld and fingerprint plots [16] for (1) are shown in Fig. 2. Hirshfeld and fingerprint plots generated, and all interactions are visible in the fingerprint plots. In the Hirshfeld surface, close contacts are visible in a red color. The fingerprint analysis of compound (1) shows that H–H interactions are responsible for around 39.5%, C–H…O for 27.6%, C–H for 23.7%, C–O for 4.6, and C–C for 4% of the close contacts in the Hirshfeld surfaces. These interactions are displayed in the fingerprint 2D plot between di (di is closest internal distance) and de (closest external distance).

Table 3 shows the results of the interaction energy calculations for (1). The strongest interaction energy involves a pair of C–H…π interactions between molecules related by a center of symmetry (Fig. 3). Another interaction of interest is these weak H-bonds (C2–H2…O2 and C3–H3…O2) that result in an $R^2_2(18)$ ring and ultimately to the sheets, as shown in Fig. 1. The third interaction explored is an intriguing π…π interaction involving the carbonyl group and the phenyl ring system. Of particular interest is the large electrostatic component calculated for this interaction, presumably a result

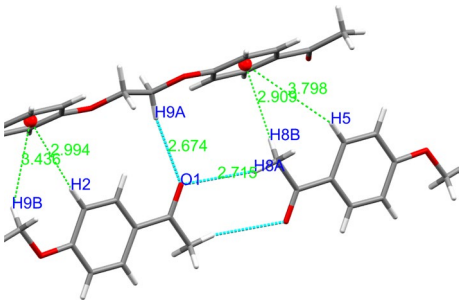

Fig. 4 Partial packing diagrams of compound (**2**) view along the b-axis. Symmetry code: 1 + *x*, *y* , −1 + *z* (H8A..O1), 1 − x, 1/2 − *y*, − 1/2 − *z*

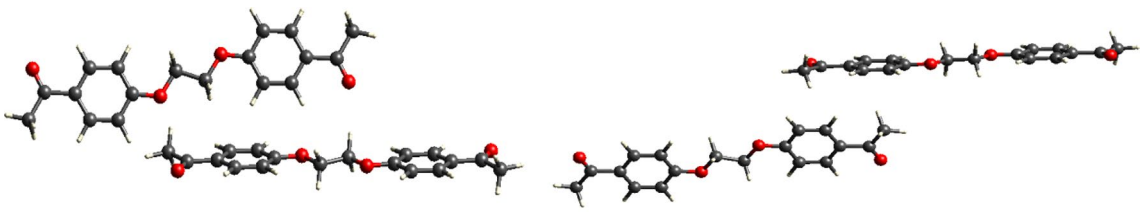

(a) **(b)**

Fig. 3 **a** C(2)–H(2)…Cg(1) [2645.01] 2.99 136 3.7231(14) [2645] = 1 − *X*, − 1/2 + *Y*, 1/2 − *Z* **b** C(8)–H(8B)…Cg(1) [2555.01] 2.91 150 3.7721(15) [2555] = − *X*, 1/2 + *Y*, 1/2 − Z

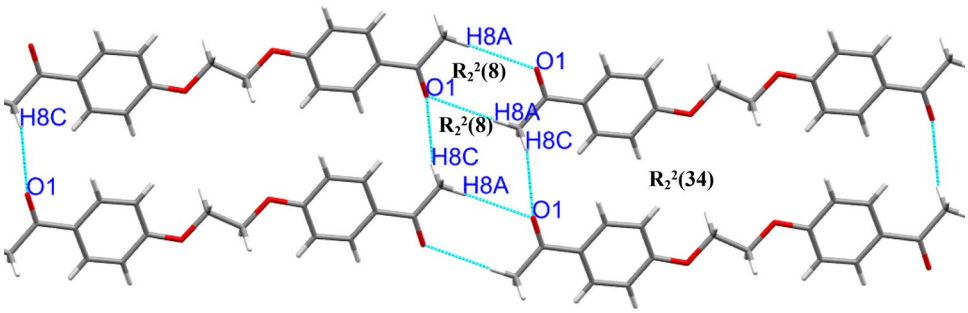

Fig. 5 Partial packing diagrams of compound (**2**) symmetry code: $1+x, y, -1+z$

Table 4 Hydrogen-bond geometry (Å) for (**2**)

D–H…A	D–H	H…A	D…A	D–H…A (°)
C8–H8a…O1$^{(i)}$	0.960	2.715	3.612	155.95
C9–H9a…O1$^{(ii)}$	0.970	2.674	3.514	145.16
C8–H8c…O1$^{(iii)}$	0.960	2.679	3.595	159.59
C2–H2… Cg (C1–C6)$^{(iv)}$	0.930	2.994	3.723	136.37
C5–H5… Cg (C1–C6)$^{(v)}$	0.930	3.798	4.611	148.87
C9–H9b… Cg (C1–C6)$^{(vi)}$	0.970	3.436	4.296	148.91

Cg is the centroid of the ring. Symmetry codes: (i) $1-x, -y, z$ (ii) $1-x, -y, z$ (iii) $x, -1/2-y, -1/2+z$ (iv) $1-x, -y, -z$ (v) $1-x, -y, -z$ (vi) $1-x, -y, 1-z$

of the charge distribution in the aldehyde functional group and the polarization of the phenyl ring by its substituents.

Compound (2) is having $COCH_3$ at the *p* position of the ring, and again like compound (1), only carbonyl oxygen is taking part in weak interactions. In an extensive hydrogen-bonding network, terminal carbonyl oxygen is involved in three weak interactions, and two were forming an eight-membered R_2^2 (8) and R_2^2 (8) ring, in which C–H–O interactions are involved. The partial packing diagram of the compound is shown in Figs. 4 and 5.

In this compound, C–H…π interactions are exhibited in the crystal packing between C5H5–Cg (C1 C2 C4 C5 C8 C9) π-electrons of the ring of the adjacent molecule (Table 4). Compound 2 is having C–H…π aromatic interactions as major non-covalent interactions, which shows the involvement of electrostatic forces rather than dispersion forces in aromatic interactions [23].

Hirshfeld and fingerprint plots [16] for (2) are shown in Fig. 6. The fingerprint analysis of compound (2) shows that H–H interactions are responsible for around 41.7%, C–H–O for 25.6%, C–H for 30.8%, O–O for 1.2 and O–C for 0.3% of the close contacts in the Hirshfeld surfaces. All interactions are visible in the fingerprint 2D plot.

The results obtained for the interaction energy calculations for (2) are shown in Table 5, in which the primary

Table 5 Interaction energies (kJ mol^{-1}) calculated for (**2**)

Interaction(s)	E'_{ele}	E'_{pol}	E'_{dis}	E'_{rep}	E_{tot}
C2–H2…Cg(1)	−12.9	−4.2	−44.2	25.8	−39.3
2 C8–H8C…O1 [R_2^2(34)]	−13.2	−3.6	−35.0	20.2	−34.5
C8–H8B…Cg(1)	−1.8	−1.2	−23.6	11.5	−16.2
2 C8–H8A…O1 [R_2^2(8)]	−8.3	−2.4	−7.3	7.7	−12.2
	−1.0	−0.1	−4.5	2.4	−3.6

Scale factors used to determine E_{tot}:k_{ele} = 1.057, k_{pol} = 0.740, k_{dis} = 0.871, and k_{rep} = 0.618 [16]. See "Hirshfeld surface, finger-plot and weak interaction energy analysis" section for calculation details

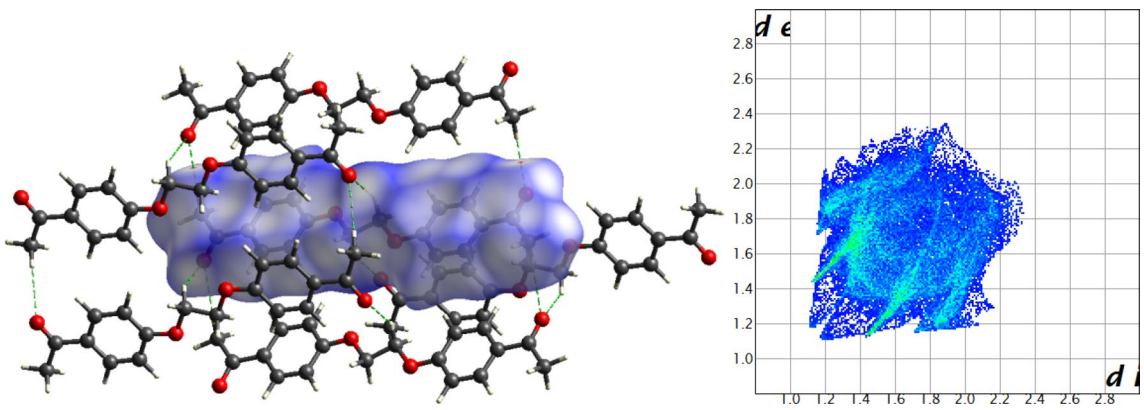

Fig. 6 Hirshfeld and fingerprint plots of compound (**2**)

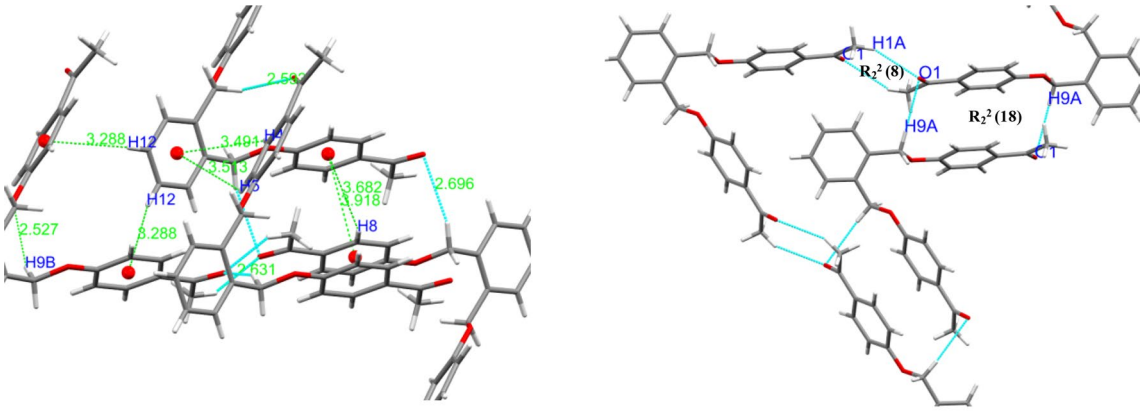

(a) (b)

Fig. 7 **a** Diagram showing the architecture of packing diagrams **b** ring motif R_2^2 (**8**) and R_2^2 (18) of compound (**3**)

Table 6 Hydrogen-bond geometry (Å) for (**3**)

D-H…A	D–H	H…A	D….A	D–H…A (°)
C9–H9a…O1$^{(i)}$	0.970	2.696	3.620	159.43
C9–H9b…O1$^{(ii)}$	0.970	2.593	3.479	151.97
C1–H1A…O1$^{(iii)}$	0.960	2.631	3.503	151.33
C8H8…Cg (C3–C8)$^{(iv)}$	0.930	3.682	3.605	77.99
C5H5… Cg (C10–C12)$^{(v)}$	0.930	3.513	3.978	113.59
C4H4… Cg (C10–C12)$^{(vi)}$	0.930	3.491	3.967	114.44
C12H12… Cg (C3–C8)	0.930	3.288	4.173	159.65
Cg (C3–C8)…. Cg (C3–C8)	–	3.918	–	–

Cg is the centroid of the ring

Symmetry codes: (i)$1/2-x, -1/2+y, 1.5-z$ (ii) $1/2-x, -1/2-y, 1-z$ (iii) $1/2-x, -1.5-y, 1-z$ (iv) $1/2+x, 1/2-y, 1/2+z$ (v) $1/2-x, 1.5-y, 1-z$ (vi) $1/2-x, 1.5-y, 1-z$

interactions are indicated for the strongest. There are no significant $\pi\ldots\pi$ interactions [the closest Cg…Cg distance is 4.9415 (8) Å]. Two C–H…pi interactions are responsible for the strongest and the third strongest interaction between molecular pairs results. A pair of weak H-bonds involving the carbonyl group results in an $R_2^2(34)$ motif and yields significant interaction energy between molecules related by a translation along the b-axis. Another set of C–H…O interactions involving the carbonyl group results in an $R_2^2(8)$ motif between inversion center-related molecules.

Compound (3) is having restrictions in the rotation due to the linked phenyl ring. The molecular structure is symmetrical in the structure, like an open book. Terminal oxygen of carbonyl is involved in an extended network structure to form R_2^2 (8) and R_2^2 (18) in ring, as shown in Fig. 7b. This oxygen is trifurcated and involved in three hydrogen bonding.

In addition to C–H–O hydrogen bonding, the extended structure of (3) in Fig. 7a exhibits C–H–π interactions (Table 6) in which C12–H12-π interaction is the result of the tilted structure of the aromatic ring concerning each other. C4–H4-π and C5–H5-π interactions are exhibited for the development of tilted structure in the crystal. Linked oxygen is involved in an extended network structure to form R_2^2 (8) and R_2^2 (18) ring (Fig. 7b). Finally, the superstructure exhibits a weak π–π interaction between adjacent molecules, with a Cg (C3–C8)…Cg (C3–C8) distance of 3.918 Å (Table 5)

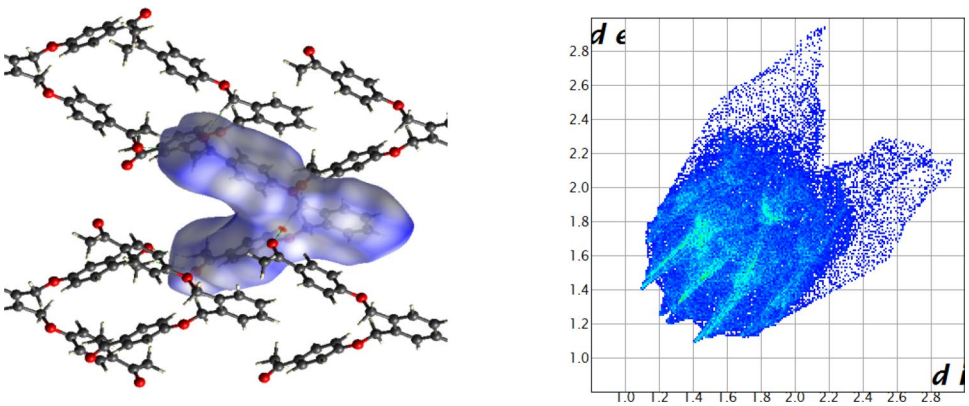

Fig. 8 Hirshfeld and fingerprint plots of compound (**3**)

Table 7 Interaction energies (kJ mol^{-1}) calculated for (**3**)

Interaction(s)	E'_{ele}	E'_{pol}	E'	E'_{rep}	E_{tot}
Cg(1)…Cg(1)/2 C9–H9…O1	−21.6	−4.7	−57.1	34.2	−54.9
C9–H9B…O1/C4–H4… Cg(2)/C5–H5…Cg(2)	−10.8	−4.0	−27.7	15.7	−28.8
	−1.1	−2.0	−36.8	21.7	−21.3
2 C12–H12…Cg(1)	−2.0	−1.4	−30.8	16.8	−19.6
	−3.0	−1.0	−21.6	7.3	−18.3
2 C1–H1A…O1 [$R_2^2(8)$]	−8.4	−2.8	−8.7	10.5	−12.1

Scale factors used to determine E_{tot}:k_{ele} = 1.057, k_{pol} = 0.740, k_{dis} = 0.871, and k_{rep} = 0.618 [16]. See "Hirshfeld surface, finger-plot and weak interaction energy analysis" section for calculation details

Hirshfeld and fingerprint plots [16] for (3) are shown in Fig. 8. The fingerprint analysis of compound (3) shows that H–H interactions are responsible for around 47%, C–H–O for 21.4%, C–H for 27.8%, and C–C for 3.9 of the close contacts in the Hirshfeld surfaces. All interactions are visible in the fingerprint 2D plot.

The results obtained for the interaction energy calculations for (3) are shown in Table 7, in which the primary interactions are indicated for the strongest. A π…π interaction between phenyl rings containing C3 through C8 (related by ½ − x, ½ − y, 1 − z) (Fig. 9a) leads to the strongest calculated interaction energy. The molecular pair also has two C9-H9A…O1 hydrogen bonds (Fig. 10a). The second strongest interaction involves molecules having a C9-H9B…O1 and two C–H…π interactions in which the π system is from the six-membered ring comprised of C10 through C12 and the donors are C4–H4 and C5–H5 (Fig. 9b).

The final interaction explored is that of two molecules participating in two C1–H1A…O1 hydrogen bonds resulting in an $R_2^2(18)$ motif. The last interaction, the one resulting in the ring formation, is the only one in which the

Fig. 9 **a** π···π interaction with symmetry code 1/2 − x, 1/2 − y, 1 − z. The interaction also includes two weak C9–H9A···O1i hydrogen bonds **b** two weak C–H···π interactions with symmetry code x, − 1 + y, z)

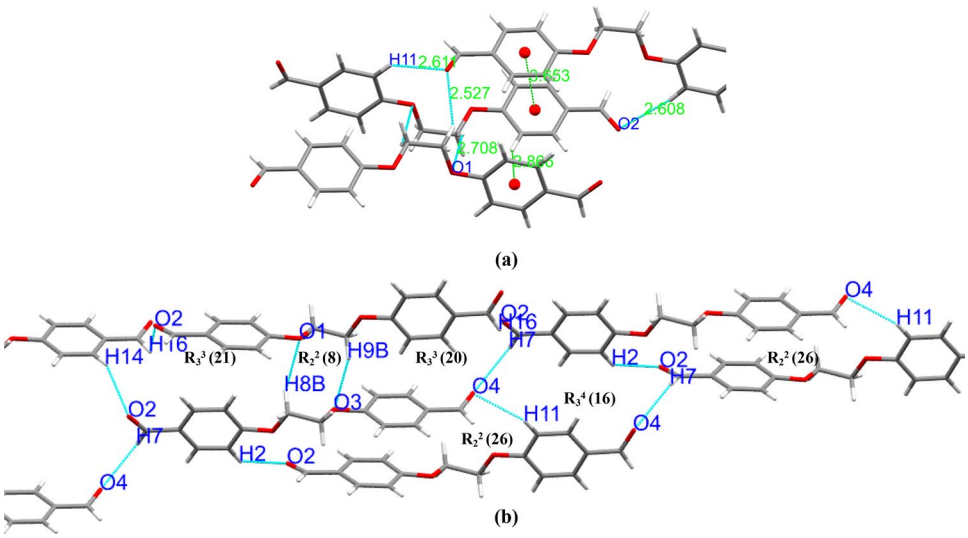

Fig. 10 **a** Partial packing diagrams along the c-axis **b** extended network of compound 4

Table 8 Hydrogen-bond geometry (Å) for (**4**)

D–H…A	D–H	H…A	D….A	D–H…A (°)
C7–H7…O4$^{(i)}$	0.950	2.658	3.317	126.96
C14–H14…O2$^{(ii)}$	0.950	2.602	3.189	120.29
C16–H16…O2$^{(iii)}$	0.950	2.656	3.079	107.57
C9–H9b…O3$^{(iv)}$	0.989	2.709	3.438	130.75
C8–H8b…O1$^{(v)}$	0.989	2.708	3.484	135.63
C8–H8a…O4$^{(vi)}$	0.990	2.527	3.387	145.15
C11–H11…O4$^{(vii)}$	0.949	2.611	3.414	142.53
C2–H2…O2$^{(viii)}$	0.950	2.608	3.425	144.35
C3–H3… Cg (C10–C15)$^{(ix)}$	0.949	2.795	3.664	152.62
C6–H6… Cg (C1–C6)$^{(x)}$	0.950	2.866	3.693	146.11
Cg (C1–C6)… Cg (C10–C15)$^{(xi)}$		3.653		

Cg is the centroid of the ring

Symmetry codes: (i) $-1+x$, y, $-2+z$ (ii) $-1+x$, y, $-1+z$ (iii)) $-1+x$, $1-y$, $-1.5+z$(iv) $-$x, $1-y$, $-1/2+z$ (v) x, $1-y$, $-1/2+z$ (vi) $-1/2+x$, ½+y, $-1+z$ (vii) $-1/2+x$, $1.5-y$, $-1/2+z$ (viii) $-1/2+x$, $1.5-y$, $-1/2+z$ (ix) x, $1-y$, $-1/2+z$ (x) x, $1-y$, $-1/2+z$ (xi) $-1/2+x$, 1.5 − y, $-1/2+z$

electrostatic energy component is comparable to the dispersive component.

Compound (4) is an asymmetrical phenyl dimer, but the orientation of the phenyl rings is not planer. The molecule is having two terminals and two linked oxygens, and all are involved in hydrogen bonding in the extended structure of the molecule, unlikely (1) and (2) molecule. Linked oxygen of compound is involved in extended network structure to form R_2^2 (8), R_3^3 (20), R_3^3 (21), R_3^4 (16) and R_2^2 (26) ring (Fig. 10b). Terminal oxygen is trifurcated and involved in the extended ring through hydrogen bonding (Table 8).

In addition to C-H–O hydrogen bonding, the extended structure of (4) exhibits C–H–π as well as π–π interactions (Table 8), in which the tilted structure of the aromatic ring with respect to each other is the result of C3–H3-π interaction (Fig. 10a). C4–H4-π and C5–H5-π interactions are also exhibited for the development of tilted geometry of aromatic ring with respect to each other in the crystal packing. This compound exhibits a weak π–π interaction between adjacent molecules, with Cg (C3–C8)….Cg (C3–C8) face to face arene–arene interactions and distance of 3.918 Å (Table 7).

Hirshfeld and fingerprint plots [16] for (4) are shown in Fig. 11. The fingerprint analysis of compound (4) shows that H–H interactions are responsible for around 38.8%, C–H–O for 28.1%, C–H for 21.7%, C–O for 3.9%, O–O for 1.3% and C–C for 6.1% of the close contacts in the Hirshfeld surfaces. All interactions are visible in the fingerprint 2D plot.

The results obtained for the interaction energy calculations for (4) are shown in Table 9, in which the primary intermolecular interactions are indicated for the strongest interaction energies. The strongest interaction energy results from a pair of molecules involved in two C–H…π interactions. A close second involves two molecules joined by two C–H…O hydrogen bonds resulting in an $R_2^2(26)$ ring and also contains a π…π interaction (Fig. 12a). The final molecular pair explored is joined by single C–H…O hydrogen (Fig. 12b). In the two strongest interactions explored, the dispersion energy component is much larger than the electrostatic energy component, consistent with the involvement of the π electrons.

Compound (5) is an unsymmetrical phenyl dimer, but orientations of the phenyl rings are very similar to compound (4). The molecule has one terminal and two linked oxygens, and all are involved in hydrogen bonding in the extended structure of the molecule, unlikely (1) and (2) molecule. Terminal oxygen is involved in an extended network structure to form the R_2^2 (10) ring. Both linked oxygens are taking part in hydrogen bonding (Table 10). The partial packing diagram of the compound is shown in Fig. 13.

Hirshfeld and fingerprint plots [16] for (4) are shown in Fig. 14. The fingerprint analysis of compound (4) shows that H–H interactions are responsible for around 41.8%, C–H–O for 21.9%, C–H for 32.9%, C–O for 2.9%, O–O for 0.1% and

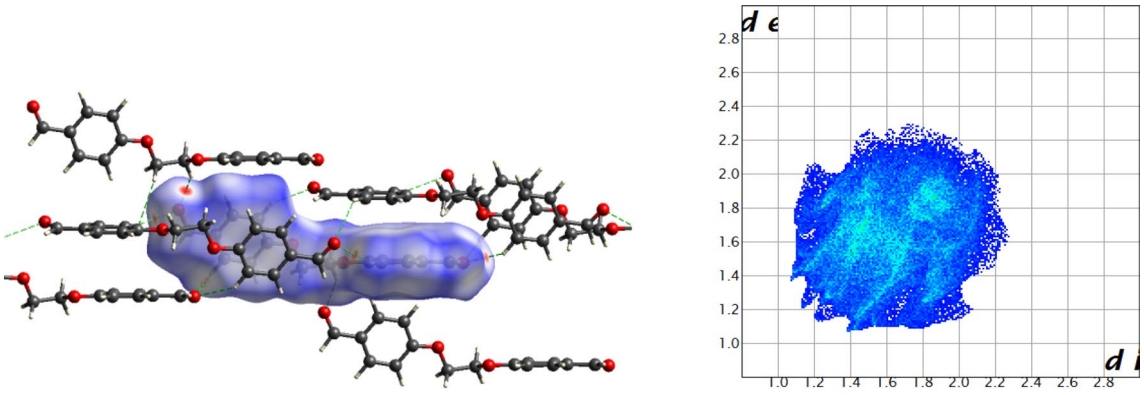

Fig. 11 Hirshfeld and fingerprint plots of compound (**4**)

Table 9 Interaction energies (kJ mol^{-1}) calculated for (**4**)

Interaction(s)	E'_{ele}	E'_{pol}	E'	E'_{rep}	E_{tot}
C6–H6…Cg(1)/ C15–H15…Cg(2)/ C9–H9B…O3/ C8–H8B…O1	−7.9	−5.2	−57.2	35.6	−40.1
Cg(1)…Cg(2)/ C2–H2…O2/ C11–H11…O4 [$R_2^2(26)$]	−12.3	−4.0	−52.8	37.2	−39.0
C8–H8A…O4	−12.9	−3.3	−16.0	13.4	−21.7
	−7.6	−2.9	−9.1	9.1	−12.5
	−6.6	−2.2	−9.5	8.5	−11.7
	−3.7	−1.1	−12.9	7.5	−11.3
	2.0	−1.4	−13.1	7.1	−6.0

Scale factors used to determine E_{tot}: $k_{ele}=1.057$, $k_{pol}=0.740$, $k_{dis}=0.871$, and $k_{rep}=0.618$ [16]. See "Hirshfeld surface, finger-plot and weak interaction energy analysis" section for calculation details

C–C for 0.3% of the close contacts in the Hirshfeld surfaces. All interactions are visible in the fingerprint 2D plot.

An analysis of close contacts reveals no significant $\pi\ldots\pi$ interactions. The results obtained for the interaction energy calculations for (5) are shown in Table 11, in which the primary intermolecular interactions are indicated for the strongest interaction energies. These interactions are containing two C–H…π interactions. A molecular pair involving a C–H…π and C–H…O bond gave the next strongest interaction. Other notable interactions explored involve C–H…O interactions, one set which results in an $R_2^2(10)$ ring motif, and a C–H…π interaction. The molecular pair in which the C–H…O interactions lead to the ring motif is the only interaction in this set in which the electrostatic energy component outweighs the dispersive component.

Aromatic interactions are present in all the compounds, mainly C–H…π interactions, but $\pi\ldots\pi$ interactions are present only in compounds 3 and 4. Compounds 1, 2 and 5 are very similar to compound 4, but non-covalent interactions are quite different irrespective of their molecular bonding. C–H…π interactions are supported by Hirshfeld surface analysis. There are prominent wings in all compound's fingerprint plot indicating the presence of C–H…π interactions. Compounds 2 and 4 are having –COCH3 group at para-position, and the rest of the molecules are having –CHO group in the ring. All compounds are having an electron-withdrawing group to polarize the electronic distribution in the ring. However, all of them are not having π–π intermolecular interaction in the opposite orientation. Some other intermolecular forces such as C–H…π, C–H…O, loan pair…π interactions re-orient the molecule and neutralize the polarization effect of CHO, COCH3 group. One common factor present in both compounds 3 and 4 is that electron-withdrawing groups are present at the para-position to the linker group. It means CHO, COCH3 at para-positions develop a uniform polarization in the ring, which suited for intermolecular $\pi\ldots\pi$ interactions.

Docking analysis was performed for synthesized compounds at the COX-2 enzyme active site and compared with standard drug SC-558. The total score obtained is shown in Table 12. The docking score (which reflects the binding capacity of drug with enzyme active site) for compound **3** was found to be **−9.95**, and for the rest of the compounds **1, 2, 4, 5** it was found to be **−7.72, −8.05, −8.1, −7.27** (Table 11). Compound 3 docking score is slightly less than that of SC-558 **(−10.78)** standard drug, suggesting that **3** (Fig. 15) can be further studied to develop a new anti-inflammatory drug.

The results of the present study have shown that compound **3** had shown to possess maximum anti-inflammatory

Table 10 Hydrogen-bond geometry (Å) for **(5)**

D–H…A	D–H	H…A	D…A	D–H…A (°)
C3–H3…O1$^{(i)}$	0.950	2.444	3.317	126.96
C13–H13…O3$^{(ii)}$	0.950	2.459	3.189	120.29
C15–H15…O2$^{(iv)}$	0.945	2.758	3.335	119.96
C2–H2….Cg (C9–C14)	0.950	2.545	4.262	134.23
C8–H8b… Cg (C1–C6)$^{(v)}$	0.990	2.692	3.495	138.48
C7–H7a… Cg (C9–C14)	0.990	3.687	3.470	69.88
C7–H7b… Cg (C9–C14)	0.991	2.551	3.470	154.13
C10–H10… Cg (C9–C14)	0.950	3.669	4.554	156.09

Cg is the centroid of the ring

Symmetry codes: (i) $-x, -1+y, z$ (ii) $2-x, 2-y, -z$ (iii) $1/2-x, 1/2+y, 1/2-z$ (iv) $1/2-x, 1/2+y, 1/2-z$ (v) $1-x, -y, -z$ (vi) $x, 1+y, z$ (v) $1/2-x, 1/2+y, 1/2-z$

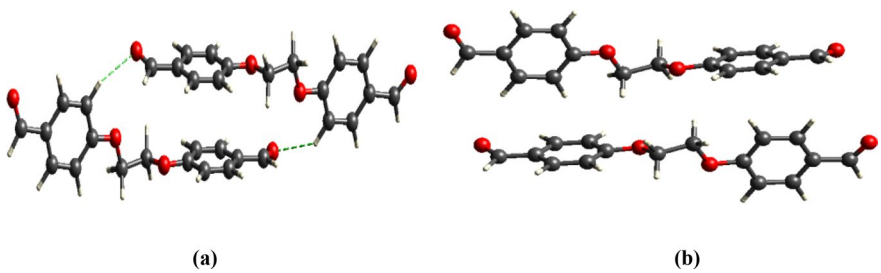

Fig. 12 **a** Cg(1)…Cg(2)^{xii} (xii = ½ + x, 3/2 − y, ½ + z) $\pi\cdots\pi$ interactions **b** C–H…[C6–H6…Cg(1)^{xiv} and C15^{xiv}–H15^{xiv}…Cg(2), where xiv = x, 1 − y, ½ + z) interactions

(a) **(b)**

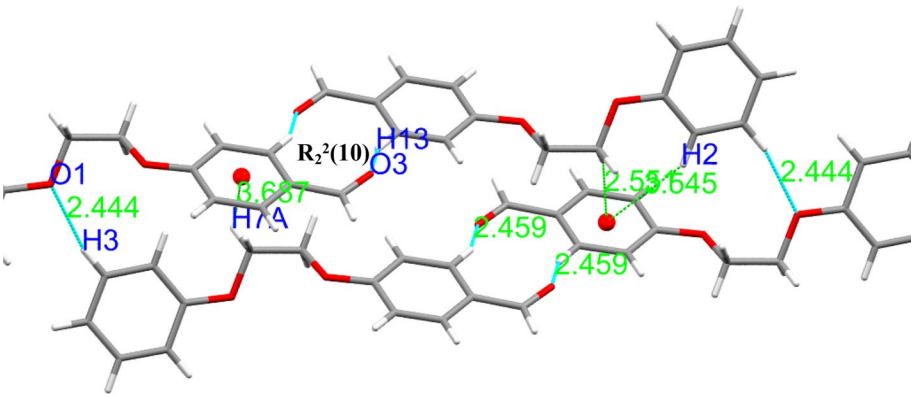

Fig. 13 Partial packing diagrams of compound (**5**) view along the b-axis

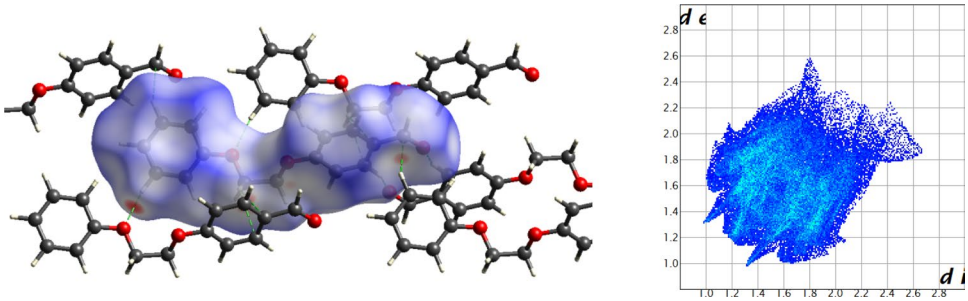

Fig. 14 Hirshfeld and fingerprint plots of compound (**5**)

Table 11 Interaction energies (kJ mol^{-1}) calculated for (**5**)

Interaction(s)	E'_{ele}	E'_{pol}	E'_{dis}	E'_{rep}	E_{tot}
2 C8–H8B…Cg(1)	−19.3	−4.4	−49.7	32.8	−46.7
C7–H7B…Cg(2)′C3–H3…O1	−14.8	−3.7	−54.6	51.0	−34.5
	−16.5	−3.6	−22.2	15.8	−29.7
C10–H10…O1/C11–H11…O2	−7.3	−1.7	−28.4	17.0	−23.2
2 C13–H13…O3 [$R_2^2(10)$]	−17.1	−5.1	−10.6	18.4	−19.7
	−2.8	−1.1	−17.4	12.3	−11.4
C15–H15…Cg(1)	−4.1	−1.0	−14.9	11.1	−11.2
	−0.7	−0.8	−13.4	11.2	−6.1
	−1.3	−0.1	−6.7	2.6	−5.7
	−2.2	−1.0	−2.8	1.8	−4.4

Scale factors used to determine E_{tot}:k_{ele} = 1.057, k_{pol} = 0.740, k_{dis} = 0.871, and k_{rep} = 0.618 [16]. See "Hirshfeld surface, finger-plot and weak interaction energy analysis" section for calculation details

effect at 180 min that is 12.7%, whereas standard drug inhibits up to 13.7% (Table 12). Other compounds, i.e., **2, 4,** and **5,** have shown intermediate effects on inhibitory properties (Tables 13, 14). Compound **1** has shown a negligible effect.

Therefore, the results indicated that structurally similar to SC-558, compound **3** is a potent inhibitor of inflammation. Torsion angle of linker oxygen atoms of compound **1, 2** is having a maximum 180°, and compound **3** linker carbons torsion angle is least 9.55°. The V shape structure of compound **3** is very similar to SC-558, which is very much suitable in binding with the active site as per docking study with COX-2. Compound **3's** flexibility is reduced by the phenyl ring to make it more compatible with binding with COX-2. Compound **3** conformations exist in V shape structure in both crystal structure as well as the most suitable conformation in docking study for binding with COX-2. This conformation favors binding with COX-2, which is observed

Table 12 Compounds docking scores, interactions compared with SC-558

Compound	Score	Hydrogen bonds	Other interactions (pi–pi stacking/hydrophobic, etc.)
(SC-558)	10.78	GLN 192	PHE 518, LEU 352, VAL 349, ARG 120, SER 353, GLY 526, VAL 523, ALA 527
1	−7.72	PHE 518, GLN 192, SER 530	SER 353, PHE 518, VAL 523, GLY 526, LEU 352
2	−8.05	PHE 518, GLN 192, TRP 387	SER 353, VAL 523, LEU 352,
3	−9.95	PHE 518	VAL 523, LEU 352, VAL 349, LEU 359, ARG 120, ALA 527, GLY 526
4	−8.1	PHE 518	SER 353, LEU 352, ALA 527, GLU 526, VAL 523
5	−7.27	PHE 518, GLN 192	SER 353, VAL 523, MET 522, TRP 387

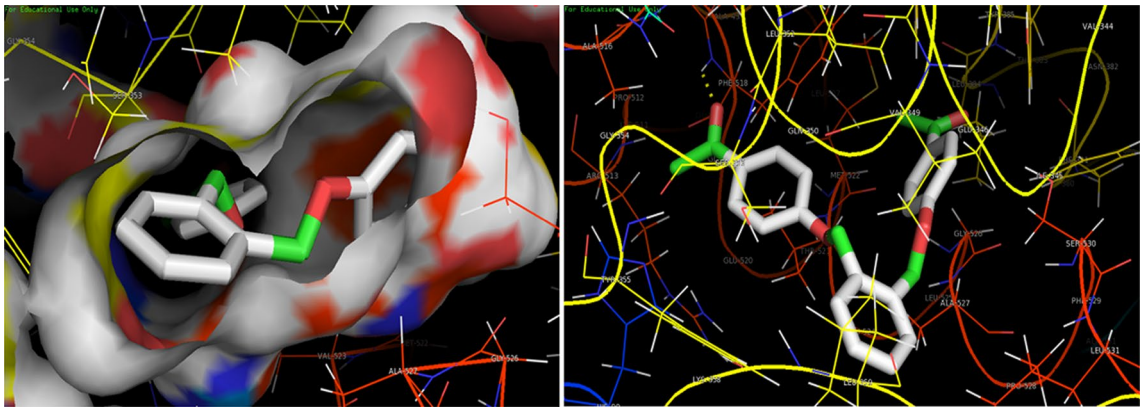

Fig. 15 Binding of compound (**3**) with COX–

Table 13 Percentage of edema growth of albino rat relative to the control group

Group	Percentage of edema growth relative to control at different time intervals (mean ± SEM)			
	0 (min)	30 (min)	90 (min)	180 (min)
Control	100 ± 0	130.2 ± 6.45 (30.2)	138.5 ± 4.45 (38.5)	122.3 ± 5.22 (22.3)
Nimu-slide	100 ± 0	113.7 ± 2.88 (13.7)	123.5 ± 3.27* (23.5)	113.7 ± 4.25 (13.7)
1	100 ± 0	116.33 ± 5.61 (16.33)	128.18 ± 3.73* (28.18)	118.17 ± 6.23 (18.17)
2	100 ± 0	116.13 ± 6.11 (16.13)	128.6 ± 4.17* (28.6)	115.19 ± 3.90 (15.19)
3	100 ± 0	113.62 ± 3.78 (13.62)	125.49 ± 7.21* (25.49)	112.7 ± 4.25 (12.7)
4	100 ± 0	117.39 ± 2.59** (17.39)	126.2 ± 3.98*** (26.2)	114.6 ± 2.54** (14.6)
5	100 ± 0	116.8 ± 5.60 (16.8)	125.6 ± 4.86 (25.6)	114.1 ± 5.86 (14.1)

$N = 6$ Number of rats in each group. Results in parentheses indicate percentage change from the respective control group

p-value < 0.05 = *; < 0.01 = **; < 0.001 = ***

Table 14 Edema growth at different intervals of albino rat

Group	Paw edema at different time intervals (ml/rat) (mean ± SEM)			
	0 (min)	30 (min)	90 (min)	180 (min)
Control	0.99 ± 0.05	1.26 ± 0.044**	1.35 ± 0.06	1.21 ± 0.072
Nimu-slide	1.02 ± 0.054	1.16 ± 0.065	1.26 ± 0.038	1.15 ± 0.045
1	1.10 ± 0.064	1.28 ± 0.058	1.41 ± 0.065	1.30 ± 0.073
2	1.12 ± 0.048	1.30 ± 0.061	1.44 ± 0.053	1.29 ± 0.062
3	1.10 ± 0.043	1.25 ± 0.048	1.38 ± 0.061	1.24 ± 0.054
4	0.92 ± 0.061	1.08 ± 0.063	1.16 ± 0.055	1.05 ± 0.067
5	1.08 ± 0.058	1.26 ± 0.059	1.35 ± 0.049	1.23 ± 0.061

Results are (mean ± SEM) of 6 rats in each group

p-value < 0.05 = *; < 0.01 = **; < 0.001 = ***

in *the* in vivo study of compound **3,** and it becomes most potent. Only small changes in **1, 2, 4**, and **5** are showing functional activity differences in a similar way as observed in the weak interactions and most stable conformations. As per the results, m-substituted phenyl rings compound **1** conformation is not well suited for binding with COX-2. The crystal structure of compound **1** shows the most stable conformation of the compound that is not similar to the most

active conformation in docking analysis. It is found in in-vivo results of compound **1,** and it becomes the least potent compound. Compounds **2, 3, 4, 5** are p-substituted phenyls rings, which enter correctly in the pocket of the COX-2 active site to make a compatible binding. Compound **2** has structural similarity with compound **1** in terms of the torsion angle of linkers, but a p-substituted ring of compound 2 makes it better than **1** to bind with COX-2. It shows that COX-2 pocket size is very much suitable for p-substituted phenyl rings. Compounds **4** and **5** docking results show that one of the –CHO groups is enough for anti-inflammatory activity. However, as per *the* in vivo study, two –CHO groups increase the activity of compound **5**. Only flexibility is not enough to make a compatible fit in the COX-2 active site. It shows that the torsion angle of the linker should be less to fit in the pocket of the COX-2 active site. So, the overall torsion angle in the crystal structure and docking study reflects the compatibility of a drug to bind with the active site.

Conclusion

Non-covalent interactions are playing a vital role in stabilizing a particular conformation of compounds. Here in these examples, intermolecular aromatic interactions are observed in unsymmetrical compound **4**. In contrast, in compounds **1** and **2**, both rings are symmetrical in their packing as well as the electronic environment in their crystals. There are small modifications in the structure of compounds by changing position and number of donor groups, but it observed that they differ a lot in its biological activity. Compound **1** is having different conformation in docking study as well as crystal structure. It shows that the crystal structure of the compound, as well as the most stable conformation of the compound, plays a significant role in its biological activity. Sometimes flexibility becomes restrictions as observed in compounds **1** and **2**, but sometimes it enhances the activity as observed in compound **3**. Both compounds **1** and **2** structural study shows a big difference with docking conformation. Both are having not good activity even they have better flexibility then compound **3**. We can conclude that only flexibility is not enough in all cases to enhance the activity. We can conclude that if structural conformation in crystal and most suitable conformations of docking analysis have similarity, then it will be more effective in biological activity. In vivo as well as in silico analysis results have a good agreement, and the only slight difference is observed in the activity of compound **5**. These are some excellent examples of fleximers to establish that weak attractive intermolecular interactions play an essential role in determining the most stable conformation of organic molecules as well as the biological activity of compounds. All these results may be helpful in drug design and the development of new materials in the field of crystal engineering.

Acknowledgements Department of Chemistry, Banaras Hindu University, Varanasi, India, is acknowledged for departmental facilities. Department of Chemistry, Mizoram University, Aizawl, Mizoram, India, is acknowledged the other infrastructure facilities. SAIF, Gauhati University, Guwahati, India, is acknowledged for SCXRD facilities. Institute of Medical Sciences, B.H.U, Varanasi, India, is acknowledged for providing the space and facilities to perform biological analysis. Jayanta Dowarah acknowledges DST, New Delhi, for DST-inspired fellowship.

Compliance with ethical standards

Conflict of interest The authors declare that they have no conflict of interest.

References

1. D.P. Marriott, I.G. Dougall, P. Meghani, Y.J. Liu, D.R. Flower, J. Med. Chem. **42**, 3210 (1999)
2. C.A. Hunter, Chem. Soc. Rev. **23**, 101 (1994)
3. R. Glaser, L.R. Dendi, N. Knotts, C.L. Barnes, Cryst. Growth Des. **3**, 291 (2003)
4. A.K. Tewari, P. Srivastava, M.C. Puerta, P. Valerga, J. Mol. Struct. **921**, 251 (2009)
5. R. Dubey, A.K. Tewari, K. Ravikumar, B. Sridhar, J. Chem. Crystallogr. **41**, 886 (2011)
6. P. Srivastava, V.P. Singh, A.K. Tewari, C. Puerta, P. Valerga, J. Mol. Struct. **1007**, 20 (2012)
7. M.R. Yadav, S.T. Shirude, A. Parmar, R. Balaraman, R. Giridhar, Chem. Heterocycl. Compd. **42**, 8 (2006)
8. R.A. Abdellatif, M.A. Chowdhury, Y. Dong, D. Das, G. Yu, C.A. Velázquez, M.R. Suresh, E.E. Knaus, Bioorg. Med. Chem. Lett. **19**(11), 3014 (2009)
9. M.H. Yang, K.D. Yoon, Y.W. Chin, J.H. Park, J. Kim, Bioorg. Med. Chem. **17**(7), 2689 (2009)
10. S.K. Rai, S. Khanam, R.S. Khanna, A.K. Tewari, Cryst. Growth Des. **15**, 1430 (2015)
11. A. Zarghi, S. Arfaei, Iran. J. Pharm. Res. **10**(4), 655 (2011)
12. A. Palomer, F. Cabre, J. Pascual, J. Campos, M.A. Trujillo, A. Entrena, M.A. Gallo, L. García, D. Mauleón, A. Espinosa, J. Med. Chem. **45**(7), 1402 (2002)
13. M. J. Turner, J. J. McKinnon, S. K. Wolff, D. J. Grimwood, P. R. Spackman, D. Jayatilaka and M. A. Spackman, CrystalExplorer17. (2017) http://crystalexplorer.scb.uwa.edu.au. Accessed 2 Apr 2019
14. S.F. Boys, F. Bernardi, Mol. Phys. **19**, 553 (1970)
15. M.J. Turner, S. Grabowsky, D. Jayatilaka, M.A. Spackman, J. Phys. Chem. Lett. **5**, 4249 (2014)
16. C.F. Mackenzie, P.R. Spackman, D. Jayatilaka, M.A. Spackman, IUCrJ **4**, 575 (2017)
17. F.H. Allen, D.G. Watson, L. Brammer, A.G. Orpen, R. Taylor, in *International Tables for Crystallography*, 3rd edn., ed. by E. Prince (Springer, Heidelberg, 2004), pp. 790–811
18. A.L. Spek, Acta Cryst. **D65**, 148 (2009)
19. R.G. Kurumbail, A.M. Stevens, J.K. Gierse, J.J. McDonald, R.A. Stegeman, J.Y. Pak, D. Glidehans, J.M. Miyashiro, T.D. Penning, K. Seibert, P.C. Isakson, W.C. Stallings, Nature **384**, 644 (1996)

20. C.A. Wintar, E.A. Risley, G.W. Nuss, Proc. Soc. Exp. Biol. **111**, 544 (1962)
21. A.K. Tewari, P. Srivastawa, V.P. Singh, A. Singh, R.K. Goel, C.G. Mohan, Chem. Pharm. Bull. **58**(5), 634 (2010)
22. R. Thakuria, N.K. Nath, B.K. Saha, Cryst. Growth Des. **19**, 523 (2019)
23. A. Banerjee, A. Saha, B.K. Saha, Cryst. Growth Des. **19**, 2245 (2019)
24. Bruker, *APEX2, SAINT and SADABS* (Bruker AXS Inc., Madison, 2015)
25. G.M. Sheldrick, Acta Cryst. **A71**, 3 (2015)
26. A.K. Tewari, V.P. Singh, M.C. Puerta, P. Valerga, Acta Cryst. **E63**, o1930 (2007)
27. P. Valerga, M.C. Puerta, CCDC 710835: Experimental Crystal Structure Determination (2016). https://doi.org/10.5517/ccdc.csd.ccrvp5f